Hindawi Publishing Corporation
Mathematical Problems in Engineering
Volume 2014, Article ID 386174, 10 pages
http://dx.doi.org/10.1155/2014/386174

Research Article

A High-Performance Control Method of Constant V/f-Controlled Induction Motor Drives for Electric Vehicles

Long Chen, Xiaodong Sun, Haobin Jiang, and Xing Xu

Automotive Engineering Research Institute, Jiangsu University, Zhenjiang 212013, China

Correspondence should be addressed to Xiaodong Sun; xdsun@ujs.edu.cn

Received 21 September 2013; Revised 12 December 2013; Accepted 12 December 2013; Published 21 January 2014

Academic Editor: Hui Zhang

A three-phase induction motor used as a propulsion system for the electric vehicle (EV) is a nonlinear, multi-input multi-output, and strong coupling system. For such a complicated model system with unmeasured and unavoidable disturbances, as well as parameter variations, the conventional vector control method cannot meet the demands of high-performance control. Therefore, a novel control strategy named least squares support vector machines (LSSVM) inverse control is presented in the paper. Invertibility of the induction motor in the constant V/f control mode is proved to confirm its feasibility. The LSSVM inverse is composed of an LSSVM approximating the nonlinear mapping of the induction motor and two integrators. The inverse model of the constant V/f-controlled induction motor drive is obtained by using LSSVM, and then the optimal parameters of LSSVM are determined automatically by applying a modified particle swarm optimization (MPSO). Cascading the LSSVM inverse with the induction motor drive system, the pseudolinear system can be obtained. Thus, it is easy to design the closed-loop linear regulator. The simulation results verify the effectiveness of the proposed method.

1. Introduction

Nowadays, some serious problems such as environment depravation and air pollution are becoming more and more serious, due to the rapid development of the global economy. Electric vehicles (EVs), including fuel cell-powered vehicle and hybrid electric vehicles, are being currently researched and their practicalities are increasingly capturing many countries' eyes, since they are a way to solve these problems that are tied to exhaust gas-emission and energy-saving issues [1–3].

By converting electrical energy into mechanical energy, a motor can propel a vehicle [4, 5]. Compared with the combustion engines, the motors have some main advantages in terms of power density, conversion efficiency, low-speed torque characteristics, and so on [6–9]. In addition, when the motor operates in the braking mode, it can convert the mechanical energy back to electrical energy [10, 11]. Aforementioned characteristics of the motors make the electric drive more energy efficient, more powerful, and more compact. With the rapid development of power electronics, information technology, and the revolution in motor control, the EV technologies are being quickly progressed. Among EV key technologies, selection of a suitable drive, optimum design of the motor topologies, and optimal control strategies are the major factors [12, 13].

In general, permanent-magnet synchronous motors (PMSMs) have been popular in EV traction applications, but some problems have recently arisen. One of the key issues is that the cost of rare earth materials, such as neodymium, has sharply increased in the past years [14–16]. Therefore, the induction motors are drawing attention as a promising alternative to PMSMs [17]. The induction motors have many characteristics, such as firm structure, small model, ruggedness, light capacity, low price, and the ability to operate in the extended high speed. Moreover, with the growth of power electronic technology and microprocess technology, high-speed induction motors driven by changeable frequency have many merits on aspects of reliability, low maintenance, low cost, craftwork, and so on [18–20]. So induction motor drive systems play an increasingly important role in driving EV. With the background, our study revisits and renews this old technology, aiming at high-performance control of the induction motor drives in EV applications.

The mature control method of induction motor drives is the vector control, which has been widely implemented in

electric drives [21, 22]. However, since the rotor flux angle of the induction motor is not directly measurable, vector control of an induction motor is more difficult than that of a PMSM. In addition, another issue in electrical drives is system sensitivity to inaccuracy and changes of motor parameters [23, 24]. Since the vector control systems are very sensitive to such inaccuracies, some parameters of the induction motor drives should be estimated online, and a more robust control structure is required. Therefore, some intelligent control methods, such as fuzzy control [25, 26], sliding mode control [27–29], adaptive control [30, 31], neural network control [32, 33], and other advanced control methods [34–36], are adopted for the induction motor drives. These approaches only improve different aspects of the control performance of induction motor drives. Thus, how to enhance the satisfying dynamic behavior of the induction motor drive for EVs further is very urgent.

The aim of this paper is to propose a novel control scheme based on least squares support vector machines (LSSVM) inverse for the constant V/f-controlled induction motor drive system for EVs. The mathematic model of the induction motor drive is presented, and a reversible analysis of such system is also performed. Based on the analysis, speed control of the induction motor drive based on LSSVM inverse system method is proposed. The method is combined by LSSVM, which has the abilities of learning and function approximation and the adaptation capacity of system parameter variations, and the inverse system method which can realize the linearization of complex nonlinear system [37, 38]. The LSSVM is used to identify the inverse model of the constant V/f-controlled induction motor drive system, and a modified particle swarm optimization (MPSO) algorithm is adopted to optimize the kernel parameter and regularization parameter of the LSSVM. Consequently, a composite pseudolinear system is completed by constructing LSSVM inverse and combining it with the original system. Then the linear control techniques can be applied to design control system to achieve the high performance control of the original nonlinear system. Finally, the simulation testing research is studied using this method, and the control effect is satisfying.

2. Mathematic Model and Reversible Analyses

For current-followed SPWM inverter of the induction motor, when the nonlinear and time delay of the inverter, magnetic saturation, and iron loss of the induction motor are ignored, the state equation is described as a 6-order nonlinear model in still α-β coordinates:

$$\begin{aligned}
\frac{d\omega_r}{dt} &= \frac{n_p}{J}\left(T_e - T_L\right) = \frac{n_p^2}{J}\left(\psi_{s\alpha} i_{s\beta} - \psi_{s\beta} i_{s\alpha}\right) - \frac{n_p}{J} T_L,\\
\frac{d\psi_{s\alpha}}{dt} &= V\cos\theta_1 - R_s i_{s\alpha},\\
\frac{d\psi_{s\beta}}{dt} &= V\sin\theta_1 - R_s i_{s\beta},\\
\frac{di_{s\alpha}}{dt} &= \frac{R_r}{L_s L_r - L_m^2}\psi_{s\alpha} + \frac{L_r}{L_s L_r - L_m^2}\omega_r \psi_{s\beta} - \frac{R_r L_s + L_r R_s}{L_s L_r - L_m^2} i_{s\alpha}\\
&\quad - \omega_r i_{s\beta} + \frac{L_r}{L_s L_r - L_m^2} V\cos\theta_1,\\
\frac{di_{s\beta}}{dt} &= \frac{R_r}{L_s L_r - L_m^2}\psi_{s\beta} - \frac{L_r}{L_s L_r - L_m^2}\omega_r \psi_{s\alpha} - \frac{R_s L_r + L_s R_r}{L_s L_r - L_m^2} i_{s\beta}\\
&\quad + \omega_r i_{s\alpha} + \frac{L_r}{L_s L_r - L_m^2} V\sin\theta_1,\\
\frac{d\theta_1}{dt} &= \omega_1,
\end{aligned} \tag{1}$$

where ω_1 and ω_r are synchronous angle frequency and rotate speed, respectively. $i_{s\alpha}$ and $i_{s\beta}$ are stator currents in α-β coordinates, respectively. $\psi_{s\alpha}$ and $\psi_{s\beta}$ are stator flux linkage in α-β coordinates, respectively. T_r is rotor time constant. L_m is mutual inductance. n_p is the number of pole pairs. L_s and L_r are stator inductance and rotor inductance, respectively. R_s and R_r are stator resistance and rotor resistance, respectively. T_e and T_L are electromagnetic torque and load torque, respectively. θ_1 is angle between the space voltage vector and the α axis. V is the amplitude of the space voltage vector.

Given the state variable

$$\mathbf{x} = \left[\omega_r, \psi_{s\alpha}, \psi_{s\beta}, i_{s\alpha}, i_{s\beta}, \theta_1\right]^T = \left[x_1, x_2, x_3, x_4, x_5, x_6\right]^T \tag{2}$$

and the input variable

$$\mathbf{u} = \left[V, \omega_1\right]^T = \left[u_1, u_2\right]^T, \tag{3}$$

the output is the ω_r, so

$$\begin{aligned}
\dot{\mathbf{x}} &= f(\mathbf{x}, \mathbf{u})\\
&= \begin{bmatrix}
\frac{n_p^2}{J}\left(x_2 x_5 - x_3 x_4\right) - \frac{n_p}{J} T_L\\
u_1\cos x_6 - R_s x_4\\
u_1\sin x_6 - R_s x_5\\
\frac{R_r}{L_s L_r - L_m^2} x_2 + \frac{L_r}{L_s L_r - L_m^2} x_1 x_3 - \frac{R_r L_s + L_r R_s}{L_s L_r - L_m^2} x_4\\
-x_1 x_5 + \frac{L_r}{L_s L_r - L_m^2} u_1\cos x_6\\
\frac{R_r}{L_s L_r - L_m^2} x_3 - \frac{L_r}{L_s L_r - L_m^2} x_1 x_2 - \frac{R_s L_r + L_s R_r}{L_s L_r - L_m^2} x_5\\
+x_1 x_4 + \frac{L_r}{L_s L_r - L_m^2} u_1\sin x_6\\
u_2
\end{bmatrix},\\
\mathbf{y} &= h(\mathbf{x}) = x_1 = \omega_r.
\end{aligned} \tag{4}$$

When the induction motor is operating in the constant V/f control mode, we can obtain the following expression:

$$V = k\omega_1, \tag{5}$$

where $k = \sqrt{3/2}\cdot(220\cdot\sqrt{2})/(2\cdot\pi\cdot 50) = ((\sqrt{3}\cdot 220)/(2\cdot\pi\cdot 50))$ is the proportion coefficient of frequency voltage.

So

$$u_1 = ku_2. \tag{6}$$

In order to analyze the reversibility of the induction motor, the output formula should be differentiated until the input variable is visualized firstly. According to expression (11), the following expressions can be deduced:

$$y^{(1)} = x^{(1)} = \frac{n_p^2}{J}\left(x_2x_5 - x_3x_4\right) - \frac{n_p}{J}T_L, \tag{7}$$

$$\begin{aligned} y^{(2)} &= \frac{n_p^2}{J}\left(x_2\dot{x}_5 + \dot{x}_2x_5 - x_3\dot{x}_4 - \dot{x}_3x_4\right) \\ &= \frac{n_p^2}{J}\left[x_2\left(\frac{R_r}{L_sL_r - L_m^2}x_3 - \frac{L_r}{L_sL_r - L_m^2}x_1x_2 \right.\right. \\ &\qquad - \frac{R_sL_r + L_sR_r}{L_sL_r - L_m^2}x_5 + x_1x_4 \\ &\qquad \left.\left. + \frac{L_r}{L_sL_r - L_m^2}ku_2\sin x_6\right) \right. \\ &\qquad + \left(ku_2\cos x_6 - R_sx_4\right)x_5 \\ &\qquad - x_3\left(\frac{R_r}{L_sL_r - L_m^2}x_2 \right. \\ &\qquad + \frac{L_r}{L_sL_r - L_m^2}x_1x_3 \\ &\qquad - \frac{R_rL_s + L_rR_s}{L_sL_r - L_m^2}x_4 - x_1x_5 \\ &\qquad \left. + \frac{L_r}{L_sL_r - L_m^2}ku_2\cos x_6\right) \\ &\qquad \left. - \left(ku_2\sin x_6 - R_sx_5\right)x_4\right], \end{aligned} \tag{8}$$

$$\begin{aligned} \frac{\partial y^{(2)}}{\partial u_2} &= \frac{n_p^2}{J}\left[x_2\frac{L_r}{L_sL_r - L_m^2}k\sin x_6 + k\cos x_6x_5 \right. \\ &\qquad \left. - x_3\frac{L_r}{L_sL_r - L_m^2}k\cos x_6 - k\sin x_6x_4\right] \\ &= \frac{n_p^2}{J}\left[\frac{L_rk}{L_sL_r - L_m^2}\left(x_2\sin x_6 - x_3\cos x_6\right) \right. \\ &\qquad \left. + k\left(\cos x_6x_5 - \sin x_6x_4\right)\right]. \end{aligned} \tag{9}$$

Since $x \in \mathbf{\Omega} = \{x \in R^6 : (L_rk/(L_sL_r - L_m^2))(x_2\sin x_6 - x_3\cos x_6) + k(x_5\cos x_6 - x_4\sin x_6) \neq 0\}$, the inverse of system is existent. According to implicit function theorem, the inverse system can be written as

$$u = \xi\left(x, y, \dot{y}, \ddot{y}\right). \tag{10}$$

3. Basic Conception of LSSVM

As an interesting variant of the standard support vector machines (SVM), least squares support vector machines (LSSVM) have been proposed by Suykens and Vandewalle for solving pattern recognition and nonlinear function estimation problems [39, 40]. Here, we simply present the basic principle of LSSVM. Considering a given training set $\{\mathbf{x}_i, \mathbf{y}_i\}_{i=1}^l$, with input data $\mathbf{x}_i \in \mathbf{R}^n$ and output data $\mathbf{y}_i \in \mathbf{R}$, in feature space, the regression model takes the form

$$f(\mathbf{x}) = \mathbf{w}^T\mathbf{\Phi}(\mathbf{x}) + b, \tag{11}$$

where the nonlinear mapping $\mathbf{\Phi}(\cdot) : \mathbf{R}^n \rightarrow \mathbf{R}^H$ maps the input data into a higher dimensional feature space, $\mathbf{w} \in \mathbf{R}^H$ is a weight vector of the same dimension as the feature space, and b is a threshold. Then the following optimization problem for the LSSVM is formulated:

$$\begin{aligned} \min \quad & J(\mathbf{w}, \xi) = \frac{1}{2}\|\mathbf{w}\|^2 + \frac{1}{2}\gamma\sum_{i=1}^{l}\xi_i^2 \\ \text{subject to} \quad & \mathbf{y}_i = w^T\mathbf{\Phi}(x_i) + b + \xi_i, \end{aligned} \tag{12}$$

where ξ is approximation error at the instant i, J is a loss function, and γ is an adjustable constant which determines penalties for estimation errors.

The corresponding Lagrange function is described as

$$\mathbf{L}(\mathbf{w}, b, \boldsymbol{\xi}, \boldsymbol{\alpha}) = J(\mathbf{w}, \boldsymbol{\xi}) - \sum_{i=1}^{l}\alpha_i\left[\mathbf{w}^T\mathbf{\Phi}(\mathbf{x}_i) + b + \boldsymbol{\xi}_i - \mathbf{y}_i\right], \tag{13}$$

where $\boldsymbol{\alpha} = (\alpha_1, \alpha_2, \alpha_3, \ldots, \alpha_l)^T$ is a vector with the Lagrange multipliers.

According to the optimization conditions by Karush-Kuhn-Tucker, the optimal values can be found by setting the derivatives of the Lagrange function equal to zero:

$$\begin{aligned} \frac{\partial\mathbf{L}}{\partial\mathbf{w}} = 0 &\longrightarrow \mathbf{w} = \sum_{i=1}^{l}\alpha_i\mathbf{\Phi}(x_i), \\ \frac{\partial\mathbf{L}}{\partial b} = 0 &\longrightarrow \sum_{i=1}^{l}\alpha_i = 0, \\ \frac{\partial\mathbf{L}}{\partial\xi_i} = 0 &\longrightarrow \alpha_i = \gamma\xi_i, \quad i = 1, 2, \ldots, l, \\ \frac{\partial\mathbf{L}}{\partial\alpha_i} = 0 &\longrightarrow \mathbf{w}^T\mathbf{\Phi}(\mathbf{x}_i) + b + \xi_i - \mathbf{y}_i = 0. \end{aligned} \tag{14}$$

Then the optimization problem can be rewritten as

$$\begin{bmatrix} 0 & \mathbf{1}_{l\times1}^T \\ \mathbf{1}_{l\times1} & \mathbf{\Omega} + \gamma^{-1}\mathbf{I} \end{bmatrix}\begin{bmatrix} b \\ \boldsymbol{\alpha} \end{bmatrix} = \begin{bmatrix} 0 \\ \mathbf{y} \end{bmatrix}, \tag{15}$$

where $\mathbf{y} = [y_1, y_2, y_3, \ldots, y_l]^T$, $\mathbf{1}_{l\times1} = [1, 1, \ldots, 1]^T$, $\mathbf{I} = \text{diag}[1, 1, \ldots, 1]$, $\mathbf{\Omega} = \{\Omega_{ij}\}_{l\times l}$, $\Omega_{ij} = \mathbf{\Phi}^T(\mathbf{x}_i)\cdot\mathbf{\Phi}(\mathbf{x}_j)$, $i = 1, 2, \ldots, l$.

According to Mercer's condition, there is kernel function $K(\mathbf{x}_i, \mathbf{x}) = \mathbf{\Phi}^T(\mathbf{x}_i)\cdot\mathbf{\Phi}(\mathbf{x})$, which causes such LSSVM model

$$f(\mathbf{x}) = \sum_{i=1}^{l}\boldsymbol{\alpha}_iK(\mathbf{x}_i, \mathbf{x}) + b, \tag{16}$$

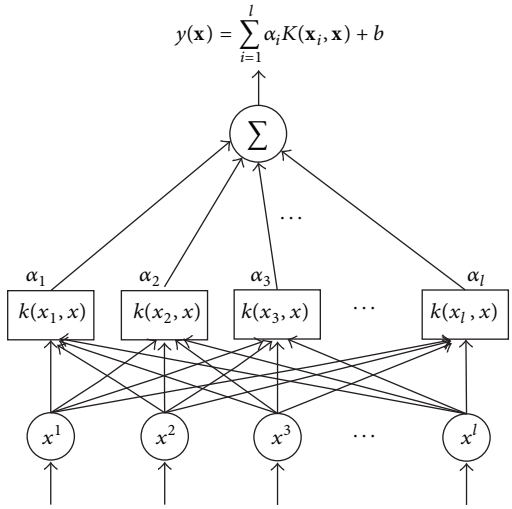

Figure 1: Structure of least squares support vector machine.

where $\boldsymbol{\alpha}$ and b are obtained by solving (7). In this paper, we will focus on RBF kernel function which corresponds to

$$K(\mathbf{x}_i, \mathbf{x}) = \exp\left(\frac{-|\mathbf{x}_i - \mathbf{x}|^2}{2\sigma^2}\right), \tag{17}$$

where σ is the kernel parameter. The structure of the LSSVM is shown in Figure 1.

4. MPSO-Based Parameters Optimization for LSSVM

4.1. MPSO. Particle swarm optimization (PSO), a novel evolutionary computation technique, was proposed by Kennedy and Eberhart in 1995 [41–43]. It is inspired by social behavior of bird flocking and fish schooling and has been found to be robust in solving nonlinear optimization problems. Compared with other stochastic approaches, PSO can generate solutions of high quality with relative shorter calculation time and has more stable convergence features. In the original PSO algorithm, particles flying through the search space are affected by two factors: one is the best position ever found of the individual, and another is the best position of the group.

The position and velocity of ith individual (called particle) in d-dimensional search space can be represented as $\mathbf{u}_i = [u_{i1}, u_{i2}, \ldots, u_{id}]$ and $\mathbf{v}_i = [v_{i1}, v_{i2}, \ldots, v_{id}]$, respectively. The local best of the ith particle can be denoted as $\mathbf{p}_i = [p_{i1}, p_{i2}, \ldots, p_{id}]$ and the global best found so far can be denoted as $\mathbf{p}_g = [p_{g1}, p_{g2}, \ldots, p_{gd}]$. Then, at each iteration, the new positions and velocities of each particle can be calculated as shown in the following formulas:

$$\begin{aligned}\mathbf{v}_i(k+1) = \omega \mathbf{v}_i(k) &+ c_1 r_1 \left(\mathbf{p}_i(k) - \mathbf{u}_i(k)\right) \\ &+ c_2 r_2 \left(\mathbf{p}_g(k) - \mathbf{u}_i(k)\right),\end{aligned} \tag{18}$$

$$\mathbf{u}_i(k+1) = \mathbf{u}_i(k) + \mathbf{v}_i(k), \tag{19}$$

where $i = 1, 2, \ldots, m$. m is the number of particles. k is the number of current iteration. $\mathbf{u}_i(k)$ is the position of ith particle at iteration k. $\mathbf{p}_i(k)$ is the best local position of ith particle at iteration k. $\mathbf{p}_g(k)$ is the best global position of all particles at iteration k. $\mathbf{v}_i(k)$ is the velocity of ith particle at iteration k. r_1 and r_2 are random variables drawn from a uniform distribution in the range $[0, 1]$ to provide a stochastic weight of the different components participating in the particle velocity definition. c_1 and c_2 are two acceleration constants regulating the relative velocities with respect to the best global and local positions, respectively. ω is the inertia weight used as a tradeoff between global and local exploration capabilities of the swarm. Let the inertia weight be a high value $\omega_{\max}$ in the early evolution and linearly decrease to $\omega_{\min}$ at the maximal number of iterations. Its mathematical representation can be described as

$$\omega = \omega_{\min} + \frac{n_{\max} - n}{n_{\max}} \left(\omega_{\max} - \omega_{\min}\right), \tag{20}$$

where $n_{\max}$ is the maximal number of iterations and n is the current number of iterations.

In order to overcome the limitation that basic PSO was not convergent because of the maximum speed parameters and big acceleration constants (c_1, c_2), Clerc introduced the shrinkage factor η. This approach can ensure that the PSO algorithm convergent during the search process. So, in this paper, we apply the MPSO method with shrinkage factor η to optimize the LSSVM's parameters. Then the mathematical representations of PSO algorithm given in (18) can be changed to

$$\begin{aligned}\mathbf{v}_i(k+1) = \eta \big(&\omega \mathbf{v}_i(k) + c_1 r_1 \left(\mathbf{p}_i(k) - \mathbf{u}_i(k)\right) \\ &+ c_2 r_2 \left(\mathbf{p}_g(k) - \mathbf{u}_i(k)\right)\big),\end{aligned} \tag{21}$$

where

$$\eta = \frac{2}{\left|2 - \varphi - \sqrt{\varphi^2 - 4\varphi}\right|}, \quad \varphi = c_1 + c_2 > 4. \tag{22}$$

Aiming at the regularization parameter γ and kernel parameter σ which are needed to be optimized, choose mean square root error (RMSE) of the LSSVM as shown in (14) as the fitness function $f(\cdot)$ of the MPSO:

$$f(\mathbf{u}) = f(\gamma, \sigma) = E_{\text{RMSE}} = \sqrt{\frac{1}{l}\sum_{i=1}^{l}\left(\mathbf{y}_i - \widehat{\mathbf{y}}_i\right)^2}, \tag{23}$$

where $\mathbf{y}_i$ and $\widehat{\mathbf{y}}_i$ are real value and model output one, respectively. The minimization of the fitness function can be seen as a mechanism to guarantee a reasonable choice of the optimized parameters (γ, σ).

4.2. Procedure of LSSVM's Parameters Optimization Using MPSO. The steps of the MPSO-LSSVM estimation are summarized as follows.

Step 1. Generate training and test samples sets, and normalize the data.

Step 2. Initialize the parameters of MPSO. The values of the parameters are as follows: $m = 60$, $d = 2$, $n_{\max} = 500$, $c_1 = c_2 = 2.05$, $\omega_{\max} = 0.9$, and $\omega_{\min} = 0.4$.

Step 3. Generate an initial swarm of size m. Set the best position of each particle with its initial position; that is, $\mathbf{p}_i = \mathbf{u}_i$ $(i = 1, 2, \ldots, m)$.

Step 4. Set to zero the velocity vectors $\mathbf{v}_i$ $(i = 1, 2, \ldots, m)$ that are associated with the m particles.

Step 5. For each candidate particle $\mathbf{u}_i$ $(i = 1, 2, \ldots, m)$, train an LSSVM estimator on the corresponding training set and with the estimation of γ and σ that are conveyed by $\mathbf{u}_i$. Then, compute its fitness function $f(\mathbf{u}_i)$.

Step 6. Update the velocity of each particle using (21). To perform the update, the best global position $\mathbf{p}_g$ is selected. $\mathbf{p}_g$ is chosen as the position exhibiting the minimal value of the considered fitness function over all explored trajectories. In detail, compare each particle's current fitness value $f(\mathbf{u}_i)$ with the fitness value of its best local position $f(\mathbf{p}_i)$. If $f(\mathbf{u}_i) < f(\mathbf{p}_i)$, let $\mathbf{p}_i = \mathbf{u}_i$. And compare the current fitness value $f(\mathbf{u}_i)$ with the fitness value of the best globe position $f(\mathbf{p}_g)$. If $f(\mathbf{u}_i) < f(\mathbf{p}_g)$, let $\mathbf{p}_g = \mathbf{u}_i$.

Step 7. Update the position of each particle by means of (19). In the event of a particle flying beyond the predefined boundary of the search space, set the position of the particle at the space boundary and reverse its search direction by means of multiplying its velocity vector by −1.

Step 8. If $n_{\max} \geq 500$ or RMSE $< 1 \times 10^{-3}$, output the optimal parameter values; else return to Step 5.

5. LSSVM Inverse Control

From the mathematical model of the constant V/f-controlled induction motor described as (2), it can be seen that the induction motor drive system is a nonlinear and strong coupling system. Therefore, it is very difficult to get the accurate analytic expression described in (10). To effectively solve this thorny problem, an LSSVM is employed to identify the inverse model of the constant V/f-controlled induction motor drive system, since the LSSVM has the ability of approaching an arbitrary nonlinear function with satisfactory accuracy. The proposed LSSVM inverse consists of an LSSVM approximating the nonlinear mapping (10) and two integrators charactering its dynamic behaviors. In view of the principle of the LSSVM regression and the control principle of the inverse system scheme, we can easily obtain the whole implementation steps of the LSSVM inverse control scheme for the induction motor drive system for EVs.

Step 1. A superposition of the random signals and constant is chosen as the input excitation signal. The original induction motor drive system is adequately excited, and then we can obtain its static and dynamic performance. We not only need the static data of the constant V/f-controlled induction motor drive system but also need the dynamic ones for the LSSVM learning the inverse model of the constant V/f-controlled induction motor. Consequently, the complete inverse model of induction motor drive system can just be gotten. During the measuring process, because there are various random noises jamming and the error of measurement devices themselves, there are generally some errors between measured values and real ones. In order to effectively overcome these disadvantages, the 2-order filters are used for adopting data. Note that the variation period of the given speed signal must be chosen properly; otherwise the practical system cannot follow the given signal. In this paper, the variation period of the all kinds of given signal is set at 10 s and the sampling period of speed is set at 0.1 s. The whole operation time is 200 s and 2000 sampled data are obtained.

Step 2. By using precise seven-point algorithm, the 1-order and 2-order offline derivative of speed output response can be obtained. Therefore, the training sample sets $\{\mathbf{x}_i, u\}$ $(i = 1, 2, \ldots, l, l = 1000)$ can be formed by chosing from original sampling period equidistantly, where, $\mathbf{x} = [y^{(2)}, y^{(1)}, y] = [\omega_r^{(2)}, \omega_r^{(1)}, \omega_r]$ and $u = \omega_1$ are, respectively, the input data and the expected output data of the LSSVM which learns the inverse model of the constant V/f-controlled induction motor drive system. Figure 2 shows the collected training data.

Step 3. According to the MPSO optimization procedure mentioned aforementioned, the best values of LSSVM parameters are $\gamma = 950$ and $\sigma = 2.6$, and its RMSE (i.e., the fitness function) is equal to 3.421×10^{-3}. Through learning the LSSVM with training sample sets, the corresponding input vector coefficient α_i (where the zero coefficients are also included in the formula) and threshold value b can be obtained. Therefore, in view of the current input $\mathbf{x}$, the output of the αth-order inversion can be identified as

$$\mathbf{u}(\mathbf{x}) = \sum_{i=1}^{d} \boldsymbol{\alpha}_i \left(\boldsymbol{\Phi}^T (\mathbf{x}_i) \cdot \boldsymbol{\Phi} (\mathbf{x}) \right) + b = \sum_{i=1}^{d} \boldsymbol{\alpha}_i K (\mathbf{x}_i, \mathbf{x}) + b. \quad (24)$$

Step 4. By combining the LSSVM inverse with the induction motor drive system, a 2-order compound system, named pseudolinear system, can be obtained as shown in Figure 3. The input and output linearization of the original constant V/f-controlled induction motor drive system is achieved. Although the relationship between input and output of the compound system is linear, there are still some nonlinear factors in the system. Therefore, the compound system is not an ideal linear system and is called the pseudolinear system. Since the compound system is an open-loop unstable system and various uncertainties are existing in practical applications, the additional closed-loop controller should be designed. In this paper, the proportional integral (PI) controller is designed for the closed-loop controller. Figure 4 shows the whole control diagram of LSSVM inverse for the induction motor drive system.

6. Simulation Test Research

The parameters of the induction motor are $P_e = 5$ KW, $R_s = 5.35\,\Omega$, $R_r = 4.85\,\Omega$, $L_s = 0.41$ H, $L_r = 0.46$ H, $L_m = 0.47$ H, and $J = 0.0018$ kg·m^2. Rated speed is 1600 r/min.

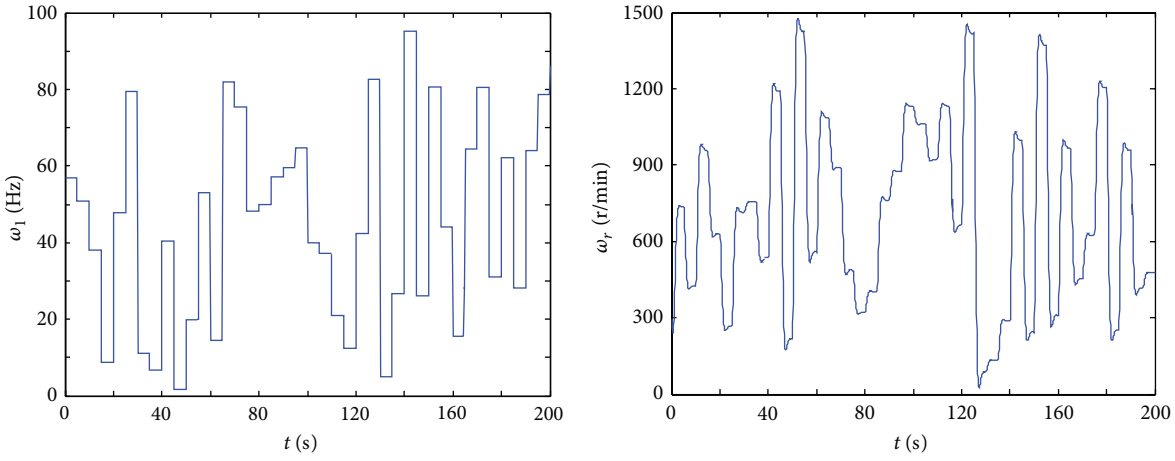

(a) ω_1 (b) ω_r

Figure 2: Collected training data.

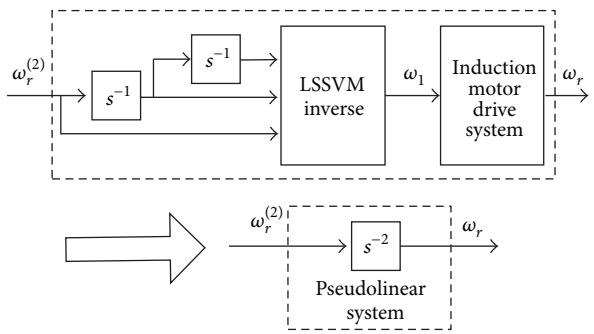

Figure 3: Diagram of pseudolinear system.

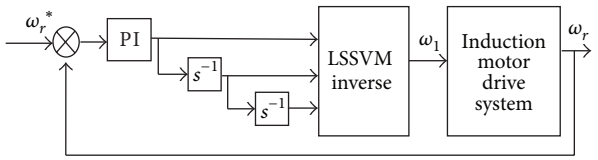

Figure 4: Control diagram of LSSVM inverse control.

6.1. Predicted Result Comparison of the Inverse Model. The remaining 1000 groups of data from the whole sample data sets are chosen and then adopted for testing sample to compare the predicted performance of the inverse model. To effectively test the performance of the inversion, the mean square root of error (E_{RMSE}) and maximal absolute error (E_{MAXE}) are considered as

$$E_{\mathrm{RMSE}} = \sqrt{\frac{1}{l}\sum_{i=1}^{l}(\mathbf{y}_i - \hat{\mathbf{y}}_i)^2}, \qquad (25)$$

$$E_{\mathrm{MAXE}} = \max_{i=1}^{l} \left|\mathbf{y}_i - \hat{\mathbf{y}}_i\right|,$$

where $i = 1, 2, \ldots, l$ and $\mathbf{y}_i$ and $\hat{\mathbf{y}}_i$ are real and predicting values.

Table 1: Comparison of predicting results of E_{RMSE}, E_{MAXE}, and t.

	E_{RMSE}	E_{MAXE}	t/s
Standard SVM	0.0091	0.0073	60. 472
Standard LSSVM	0.0053	0.0042	23. 193
MPSO-LSSVM	$1.306e-04$	$7.616e-04$	11.178

In order to verify the predicted performance of the LSSVM inversion with the MPSO algorithm (MPSO-LSSVM), the standard SVM and LSSVM are utilized for the training sample to develop the inversion of the constant V/f-controlled induction motor drive system. The CPU runtime (t/s) and the corresponding key performance indicators (E_{RMSE} and E_{MAXE}) of the models are listed in Table 1. From Table 1, it can be seen that the generalization ability and predicted precision of MPSO-LSSVM inversion is superior to the standard SVM and LSSVM inversion.

6.2. Simulation Results Analysis. The constant V/f-controlled induction motor drive system under the control schemes of the proposed method and vector control are simulated using Matlab/Simulink.

Case 1 (performance comparison of speed startup response without load disturbances). In this case, Figures 5 and 6 are, respectively, the simulation results of speed startup response curves in the case of rated load with the proposed method and vector control. The dashed and solid lines are, respectively, the reference value and practical one. Compared with the speed response with vector control, the speed response under LSSVM inverse control has a shorter settling time and much smaller overshoot and steady-state error. The corresponding performance index of the speed response is shown in Table 2. From Figures 5 and 6 and Table 2, we can see that the constant V/f-controlled induction motor drive system has a better speed-adjusting performance by using the proposed method.

Case 2 (performance comparison of tracking triangular wave without load disturbances). In this case, Figures 7 and 8

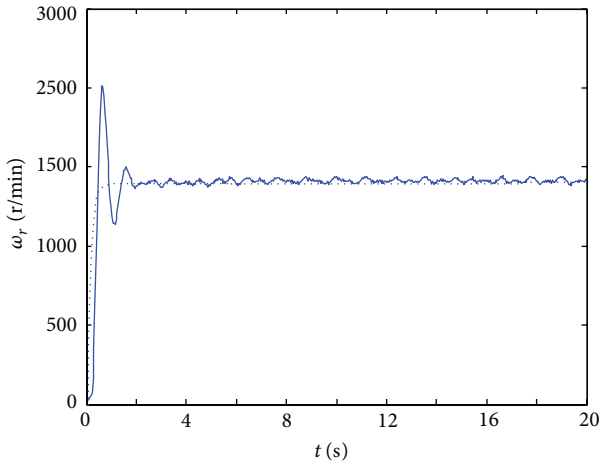

Figure 5: Speed startup response curves in the case of rated load with vector control method.

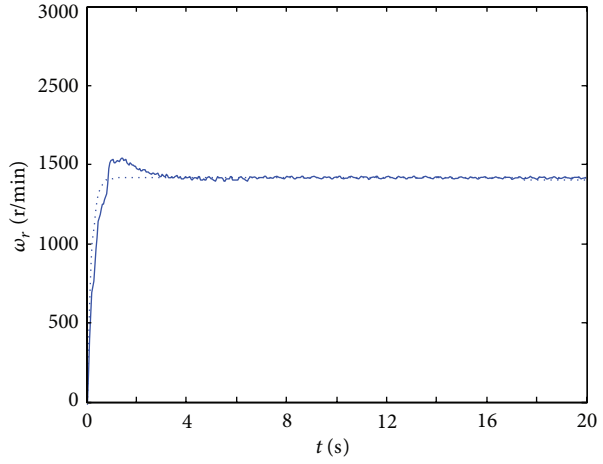

Figure 6: Speed startup response curves in the case of rated load with the proposed control method.

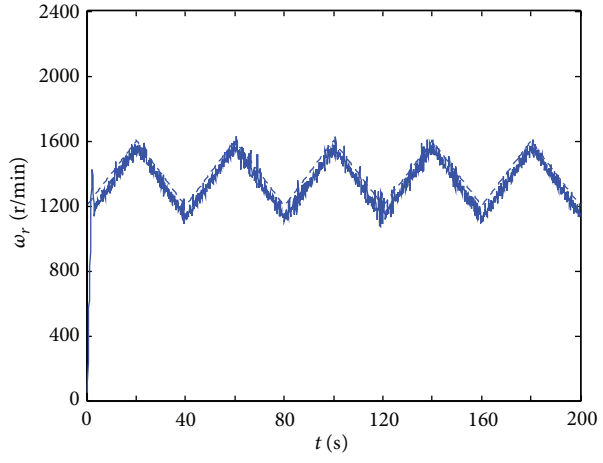

Figure 7: Response of tracking triangle curves in the case of rated load with vector control method.

Table 2: Speed performance comparison in the case of rated load.

	Settling time	Overshoot	Steady-state error
Proposed method	1.4 s	7.33%	0.56
Vector control method	2 s	32.62%	6.83

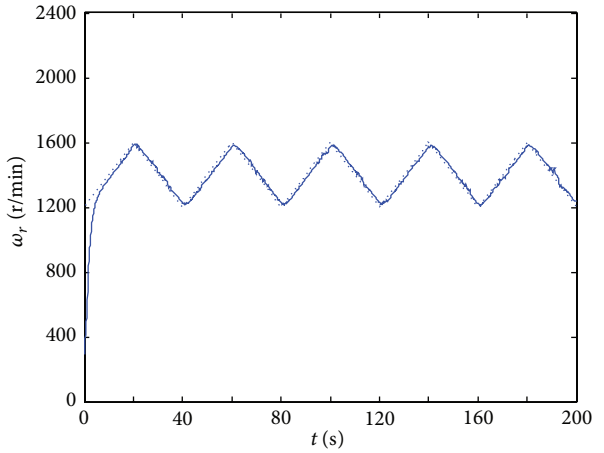

Figure 8: Response of tracking triangle curves in the case of rated load with proposed control method.

show, respectively, the simulation results of tracking triangular wave in the case of rated load with LSSVM inverse control and vector control methods. In Figures 7 and 8, the amplitudes of the triangular waves are all between 1200 r/min and 1600 r/min, and the dashed and the solid lines are, respectively, the given motor input signals and response curves. From Figures 7 and 8, we can see that, by adopting LSSVM inverse control method, the setting time of the constant V/f-controlled induction motor drive system is shorter, and its dynamic performance is also better. Additionally, the response curve can more accurately and quickly track the given motor input signal, and the control accuracy can be improved form 86% to 96%.

Case 3 (performance comparison with rotor resistance variation). Of all the motor parameters, the rotor resistance has the greatest impact on the control performance of the motor drive system. In this case, a random variable is added to the rated value of the motor rotor resistance, and its amplitude is not more than 10% of the rated resistance value. The comparison results of the proposed LSSVM inverse control and the vector control methods in the case of rotor resistance variation and without load disturbances are shown in Figures 9 and 10, respectively. From Figures 9 and 10, it can be seen that, compared with the vector control method, the LSSVM inverse scheme has a smoother speed curve with almost no overshoot. In addition, by adopting the proposed LSSVM inverse method, the relative steady error can be reduced from 12% to 4%.

Case 4 (performance comparison with load disturbances). To compare the capacity of being insensitive to the load torque variation of the proposed LSSVM inverse control and the vector control schemes, the simulation comparison

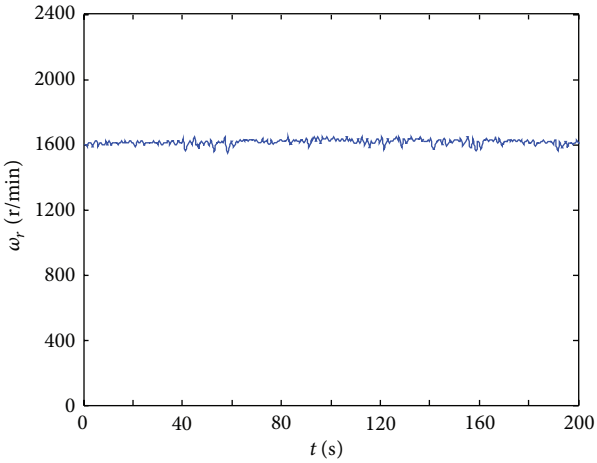

Figure 9: Speed response curves in the case of rotor resistance variation with vector control method.

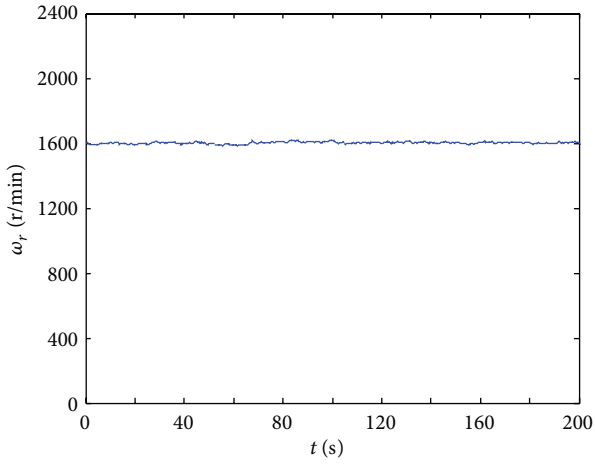

Figure 10: Speed response curves in the case of rotor resistance variation with the proposed control method.

was also carried out under sudden load disturbance impact. When the constant V/f-controlled induction motor drive system is running at steady state of 1600 r/min, a sudden load torque disturbance was applied at 100 s and removed immediately, and the simulation results of speed response curves during the sudden application and removal of the load disturbance are shown in Figures 11 and 12. From Figures 11 and 12, it can be seen that the speed response by using the proposed method recovers faster when the load torque disturbance was added and removed. We can see that the proposed method can effectively attenuate the speed deviation caused by load disturbances and has a shorter recovery time. Moreover, from Figures 11 and 12, we can see that the control accuracy can be improved form 90% to 97% by using the proposed method. Therefore, it obviously suggests that the constant V/f-controlled induction motor drive system has better robustness performance compared with the vector control method and that the LSSVM inverse method possesses a good adaptation and a much better dynamic performance against load disturbance.

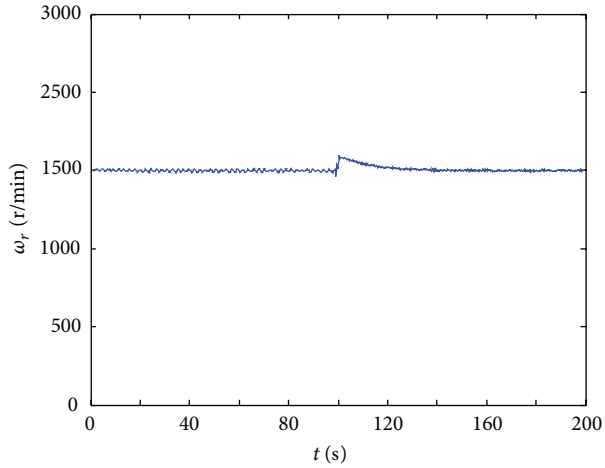

Figure 11: Speed response curves in the case of load disturbance with vector control method.

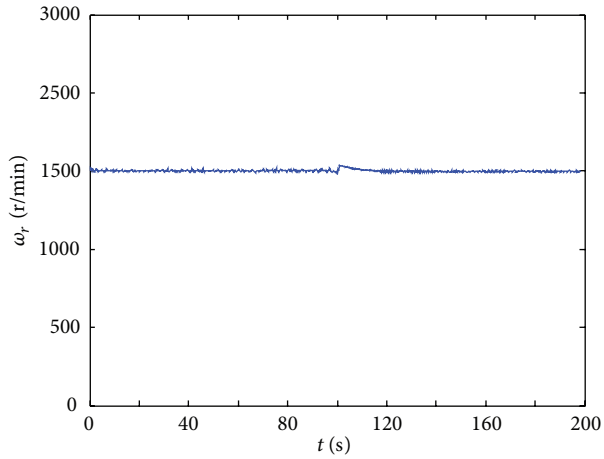

Figure 12: Speed response curves in the case of load disturbance with the proposed control method.

7. Conclusion

This paper aims at how to further improve the performance of the induction motor drive system used in EVs widely. The design and implementation procedure of a control scheme named LSSVM inverse control for a high-performance induction motor drive system for the traction purpose of EVs has been investigated. According to the characteristic of the constant V/f control mode, the mathematic model of the induction motor drive system is deduced and an inverse system model suitable for the constant V/f control mode is also obtained. Based on these, the LSSVM inverse control method is applied to control the induction motor drive system. The simulation test results testify that the proposed method is feasible and it can realize the high performance control of the induction motor drive system. It also offers a new method for the control of the induction motor drive system.

Conflict of Interests

The authors declare that there is no conflict of interests regarding the publication of this paper.

Acknowledgments

This work was supported by the National Natural Science Foundation of China under Project 51305170 and 51105177, the National New Energy Vehicle Industry Technological Innovation Plan of China (Chery Plug-in Hybrid Vehicle Industrialization Development Project), the National High Tech Research and Development Plan of China under Project SS2012AA111401, the National Science Foundation of Jiangsu Province of China under Project BK20130515 and BK20131255, the China Postdoctoral Science Foundation funded project under Project 2012M521012, the Professional Research Foundation for Advanced Talents of Jiangsu University under Project 12JDG057 and 11JDG047, and a Project Funded by the Priority Academic Program Development of Jiangsu Higher Education Institutions under Project 201106.

References

[1] K. Nam, S. Oh, H. Fujimoto, and Y. Hori, "Estimation of sideslip and roll angles of electric vehicles using lateral tire force sensors through RLS and kalman filter approaches," *IEEE Transactions on Industrial Electronics*, vol. 60, pp. 988–1000, 2013.

[2] S. Kelouwani, K. Agbossou, Y. Dubee, and L. Boulon, "Fuel cell plug-in hybrid electric vehicle anticipatory and real-time blended-mode energy management for battery life preservation," *Journal of Power Sources*, vol. 221, pp. 406–418, 2013.

[3] C. C. Chan, "The state of the art of electric and hybrid vehicles," *Proceedings of the IEEE*, vol. 90, no. 2, pp. 247–275, 2002.

[4] Z. Mei and J. Chen, "Modified motor vehicles travel speed models on the basis of curb parking setting under mixed traffic flow," *Mathematical Problems in Engineering*, vol. 2012, Article ID 351901, 14 pages, 2012.

[5] Y. Zhou, J. Lian, T. Ma, and W. Wang, "Design for motor controller in hybrid electric vehicle based on vector frequency conversion technology," *Mathematical Problems in Engineering*, vol. 2010, Article ID 627836, 13 pages, 2010.

[6] J. Vittek and S. Ryvkin, "Decomposed sliding mode control of the drive with interior permanent magnet synchronous motor and flexible coupling," *Mathematical Problems in Engineering*, vol. 2013, Article ID 680376, 17 pages, 2013.

[7] W. Chen, Y. Wu, R. Du, Q. Chen, and X. Wu, "Speed tracking and synchronization of a dual-motor system via second order sliding mode control," *Mathematical Problems in Engineering*, vol. 2013, Article ID 919837, 10 pages, 2013.

[8] J. He and C. Zhang, "A design method for fault reconfiguration and fault-tolerant control of a servo motor," *Mathematical Problems in Engineering*, vol. 2013, Article ID 647571, 6 pages, 2013.

[9] H. Zhang, Y. Shi, and A. Saadat Mehr, "Robust static output feedback control and remote PID design for networked motor systems," *IEEE Transactions on Industrial Electronics*, vol. 58, no. 12, pp. 5396–5405, 2011.

[10] A. Emadi, Y. J. Lee, and K. Rajashekara, "Power electronics and motor drives in electric, hybrid electric, and plug-in hybrid electric vehicles," *IEEE Transactions on Industrial Electronics*, vol. 55, no. 6, pp. 2237–2245, 2008.

[11] K. T. Chau, C. C. Chan, and C. Liu, "Overview of permanent-magnet brushless drives for electric and hybrid electric vehicles," *IEEE Transactions on Industrial Electronics*, vol. 55, no. 6, pp. 2246–2257, 2008.

[12] Z. Q. Zhu and D. Howe, "Electrical machines and drives for electric, hybrid, and fuel cell vehicles," *Proceedings of the IEEE*, vol. 95, no. 4, pp. 746–765, 2007.

[13] K. M. Rahman, B. Fahimi, G. Suresh, A. V. Rajarathnam, and M. Ehsani, "Advantages of switched reluctance motor applications to EV and HEV: design and control issues," *IEEE Transactions on Industry Applications*, vol. 36, no. 1, pp. 111–121, 2000.

[14] A. Akrad, M. Hilairet, and D. Diallo, "Design of a fault-tolerant controller based on observers for a PMSM drive," *IEEE Transactions on Industrial Electronics*, vol. 58, no. 4, pp. 1416–1427, 2011.

[15] T. D. Batzel and K. Y. Lee, "Electric propulsion with sensorless permanent magnet synchronous motor: implementation and performance," *IEEE Transactions on Energy Conversion*, vol. 20, no. 3, pp. 575–583, 2005.

[16] C.-F. Huang, J.-S. Lin, T.-L. Liao, C.-Y. Chen, and J.-J. Yan, "Quasi-sliding mode control of chaos in permanent magnet synchronous motor," *Mathematical Problems in Engineering*, vol. 2011, Article ID 964240, 10 pages, 2011.

[17] S. A. Taher and M. Malekpour, "A novel technique for rotor bar failure detection in single-cage induction motor using FEM and MATLAB/SIMULINK," *Mathematical Problems in Engineering*, vol. 2011, Article ID 620689, 14 pages, 2011.

[18] M. Zeraoulia, M. E. H. Benbouzid, and D. Diallo, "Electric motor drive selection issues for HEV propulsion systems: a comparative study," *IEEE Transactions on Vehicular Technology*, vol. 55, no. 6, pp. 1756–1764, 2006.

[19] T. F. Podlesak, D. C. Katsis, P. W. Wheeler, J. C. Clare, L. Empringham, and M. Bland, "A 150-kVA vector-controlled matrix converter induction motor drive," *IEEE Transactions on Industry Applications*, vol. 41, no. 3, pp. 841–847, 2005.

[20] D. Diallo, M. E. H. Benbouzid, and A. Makouf, "A fault-tolerant control architecture for induction motor drives in automotive applications," *IEEE Transactions on Vehicular Technology*, vol. 53, no. 6, pp. 1847–1855, 2004.

[21] P. Wójcik and M. P. Kaźmierkowski, "Simple direct flux vector control with space vector modulation for pwm inverter fed induction motor drive," *Przeglad Elektrotechniczny*, vol. 86, no. 2, pp. 60–64, 2010.

[22] C. Chakraborty and Y. Hori, "Fast efficiency optimization techniques for the indirect vector-controlled induction motor drives," *IEEE Transactions on Industry Applications*, vol. 39, no. 4, pp. 1070–1076, 2003.

[23] Y.-S. Jeong and J.-Y. Lee, "Parameter identification of an induction motor drive with magnetic saturation for electric vehicle," *Journal of Power Electronics*, vol. 11, no. 4, pp. 418–423, 2011.

[24] S. Cheng, P. Zhang, and T. G. Habetler, "An impedance identification approach to sensitive detection and location of stator turn-to-turn faults in a closed-loop multiple-motor drive," *IEEE Transactions on Industrial Electronics*, vol. 58, no. 5, pp. 1545–1554, 2011.

[25] M. E. H. Benbouzid, D. Diallo, M. Zeraoulia, and F. Zidani, "Active fault-tolerant control of induction motor drives in EV and HEV against sensor failures using a fuzzy decision system," *International Journal of Automotive Technology*, vol. 7, no. 6, pp. 729–739, 2006.

[26] P. Khatun, C. M. Bingham, N. Schofield, and P. H. Mellor, "Application of fuzzy control algorithms for electric vehicle antilock braking/traction control systems," *IEEE Transactions on Vehicular Technology*, vol. 52, no. 5, pp. 1356–1364, 2003.

[27] A. Nasri, A. Hazzab, I. K. Bousserhane, S. Hadjeri, and P. Sicard, "Fuzzy-sliding mode speed control for two wheels electric vehicle drive," *Journal of Electrical Engineering and Technology*, vol. 4, no. 4, pp. 499–509, 2009.

[28] A. B. Proca, A. Keyhani, and J. M. Miller, "Sensorless sliding-mode control of induction motors using operating condition dependent models," *IEEE Transactions on Energy Conversion*, vol. 18, no. 2, pp. 205–212, 2003.

[29] H. Zhang, J. Wang, and Y. Shi, "Robust H_∞ sliding-mode control for Markovian jump systems subject to intermittent observations and partially known transition probabilities," *Systems & Control Letters*, vol. 62, no. 12, pp. 1114–1124, 2013.

[30] B. Tabbache, A. Kheloui, and M. E. H. Benbouzid, "An adaptive electric differential for electric vehicles motion stabilization," *IEEE Transactions on Vehicular Technology*, vol. 60, no. 1, pp. 104–110, 2011.

[31] F. R. Salmasi, T. A. Najafabadi, and P. J. Maralani, "An adaptive flux observer with online estimation of dc-link voltage and rotor resistance for VSI-Based induction motors," *IEEE Transactions on Power Electronics*, vol. 25, no. 5, pp. 1310–1319, 2010.

[32] F.-J. Lin, Y.-C. Hung, J.-C. Hwang, I.-P. Chang, and M.-T. Tsai, "Digital signal processor-based probabilistic fuzzy neural network control of in-wheel motor drive for light electric vehicle," *IET Electric Power Applications*, vol. 6, no. 2, pp. 47–61, 2012.

[33] B. Singh, P. Jain, A. P. Mittal, and J. R. P. Gupta, "Torque ripples minimization of DTC IPMSM drive for the EV propulsion system using a neural network," *Journal of Power Electronics*, vol. 8, no. 1, pp. 23–34, 2008.

[34] H. Zhang, Y. Shi, and M. Liu, "H-infinity step tracking control for networked discrete-time nonlinear systems with integral and predictive actions," *IEEE Transactions on Industrial Informatics*, vol. 9, pp. 337–345, 2013.

[35] H. Zhang, Y. Shi, and J. Wang, "Observer-based tracking controller design for networked predictive control systems with uncertain Markov delays," *International Journal of Control*, vol. 86, pp. 1824–1836, 2013.

[36] W. Li, Y. Xu, and H. Li, "Robust $l_2 - l_\infty$ filtering for takagi-sugeno fuzzy systems with norm-bounded uncertainties," *Discrete Dynamics in Nature and Society*, vol. 2013, Article ID 979878, 8 pages, 2013.

[37] J. A. K. Suykens, J. Vandewalle, and B. De Moor, "Optimal control by least squares support vector machines," *Neural Networks*, vol. 14, no. 1, pp. 23–35, 2001.

[38] T. Van Gestel, J. A. K. Suykens, D.-E. Baestaens et al., "Financial time series prediction using least squares support vector machines within the evidence framework," *IEEE Transactions on Neural Networks*, vol. 12, no. 4, pp. 809–821, 2001.

[39] Z. Y. Han, Y. Liu, J. Zhao, and W. Wang, "Real time prediction for converter gas tank levels based on multi-output least square support vector regressor," *Control Engineering Practice*, vol. 20, pp. 1400–1409, 2012.

[40] X. B. Chen, J. Yang, J. Liang, and Q. L. Ye, "Recursive robust least squares support vector regression based on maximum correntropy criterion," *Neurocomputing*, vol. 97, pp. 63–73, 2012.

[41] I. C. Trelea, "The particle swarm optimization algorithm: convergence analysis and parameter selection," *Information Processing Letters*, vol. 85, no. 6, pp. 317–325, 2003.

[42] M. Clerc and J. Kennedy, "The particle swarm-explosion, stability, and convergence in a multidimensional complex space," *IEEE Transactions on Evolutionary Computation*, vol. 6, no. 1, pp. 58–73, 2002.

[43] H. Yoshida, K. Kawata, Y. Fukuyama, S. Takayama, and Y. Nakanishi, "A Particle swarm optimization for reactive power and voltage control considering voltage security assessment," *IEEE Transactions on Power Systems*, vol. 15, no. 4, pp. 1232–1239, 2000.